JBC ARTICLE

4-Methylumbelliferyl glucuronide contributes to hyaluronan synthesis inhibition

Nadine Nagy[‡1], Irina Gurevich[§], Hedwich F. Kuipers[‡], Shannon M. Ruppert[‡], Payton L. Marshall[‡], Bryan J. Xie[‡], Wenchao Sun[¶], Andrey V. Malkovskiy[¶], Jayakumar Rajadas[¶], Maria Grandoch[‖], Jens W. Fischer[‖], Adam R. Frymoyer[**], Gernot Kaber[‡], and Paul L. Bollyky[‡]

From the ‡Division of Infectious Diseases and Geographic Medicine, Department of Medicine, Stanford University School of Medicine, Stanford, California 94305, §Department of Dermatology, Stanford University School of Medicine, Stanford, California 94305, ¶Biomaterials and Advanced Drug Delivery (BioADD) Laboratory, Stanford University School of Medicine, Palo Alto, California 94304, ‖Pharmacology and Clinical Pharmacology, University Clinics Düsseldorf, Universitaetsstrasse 1, 40225 Düsseldorf, Germany, and **Department of Pediatrics, Stanford University School of Medicine, Palo Alto, California 94304

Edited by Peter Cresswell

4-Methylumbelliferone (4-MU) inhibits hyaluronan (HA) synthesis and is an approved drug used for managing biliary spasm. However, rapid and efficient glucuronidation is thought to limit its utility for systemically inhibiting HA synthesis. In particular, 4-MU in mice has a short half-life, causing most of the drug to be present as the metabolite 4-methylumbelliferyl glucuronide (4-MUG), which makes it remarkable that 4-MU is effective at all. We report here that 4-MUG contributes to HA synthesis inhibition. We observed that oral administration of 4-MUG to mice inhibits HA synthesis, promotes FoxP3^{+} regulatory T-cell expansion, and prevents autoimmune diabetes. Mice fed either 4-MUG or 4-MU had equivalent 4-MU:4-MUG ratios in serum, liver, and pancreas, indicating that 4-MU and 4-MUG reach an equilibrium in these tissues. LC–tandem MS experiments revealed that 4-MUG is hydrolyzed to 4-MU in serum, thereby greatly increasing the effective bioavailability of 4-MU. Moreover, using intravital 2-photon microscopy, we found that 4-MUG (a nonfluorescent molecule) undergoes conversion into 4-MU (a fluorescent molecule) and that 4-MU is extensively tissue bound in the liver, fat, muscle, and pancreas of treated mice. 4-MUG also suppressed HA synthesis independently of its conversion into 4-MU and without depletion of the HA precursor UDP-glucuronic acid (GlcUA). Together, these results indicate that 4-MUG both directly and indirectly inhibits HA synthesis and that the effective bioavailability of 4-MU is higher than previously thought. These findings greatly alter the experimental and therapeutic possibilities for HA synthesis inhibition.

Hyaluronan (HA)[2] is an extracellular matrix glycosaminoglycan with many roles in normal tissue function and development (1–3). HA is synthesized by three hyaluronan synthase (HAS) enzymes, HAS1, HAS2, and HAS3 (4). These enzymes lengthen HA by repeatedly adding glucuronic acid (GlcUA) and N-acetylglucosamine (GlcNAc) to the nascent polysaccharide as it is extruded through the cell membrane into the extracellular space (4).

There is substantial experimental and therapeutic interest in inhibiting HA synthesis. HA is known to promote inflammatory responses (2), including the activation and maturation of multiple immune cell types (5), the release of pro-inflammatory chemokines and cytokines (6, 7), and the proliferation (8) and migration (9) of leukocytes. HA and its receptor interactions are also known to influence both the number and function of lymphocytes (10–12). HA levels are greatly elevated in chronically inflamed tissues (13–15) including in the tumor microenvironment, in fibrosis, and at sites of autoimmunity (16, 17). Numerous studies by our group and others implicate HA as a driving factor in inflammation (18–20). These signals may be particularly relevant in settings of sterile inflammation such as cancer and autoimmunity (21). At most sites of injury, HA is rapidly cleared. However, at sites of autoimmunity like type 1 diabetes (T1D), HA persists (22). This may have important consequences for local immune regulation, as reviewed elsewhere (16, 23–28).

4-methylumbelliferone (4-MU) is a small molecule inhibitor of HA synthesis (29). 4-MU inhibits HA production in multiple cell lines and tissue types both in vitro and in vivo (20, 30, 31). The mechanism of action by which 4-MU inhibits HA synthesis has been described. UDP-GlcUA and UDP-GlcNAc are the substrates of the HA synthesis; their availability thereby limits HA synthesis. 4-MU functions mainly by the down-regulating of HAS expression by depleting the HA precursor UDP-GlcUA by activation of UDP-glucuronyl transferases (UGTs) (32). In addition, 4-MU

[2] The abbreviations used are: HA, hyaluronan; HAS, hyaluronan synthase; GlcUA, glucuronic acid; GlcNAc, N-acetylglucosamine; T1D, type 1 diabetes; 4-MU, 4-methylumbelliferone; 4-MUG, 4-methylumbelliferyl glucuronide; UGT, UDP-glucuronyl transferases; GAG, glycosaminoglycan; DMMB, dimethylmethylene blue; ROS, reactive oxygen species; UDPGA, UDP-glucuronic acid; DORmO, DO11.10xRIPmOVA (mouse); IS, internal standard; RT-qPCR, real-time quantitative PCR.
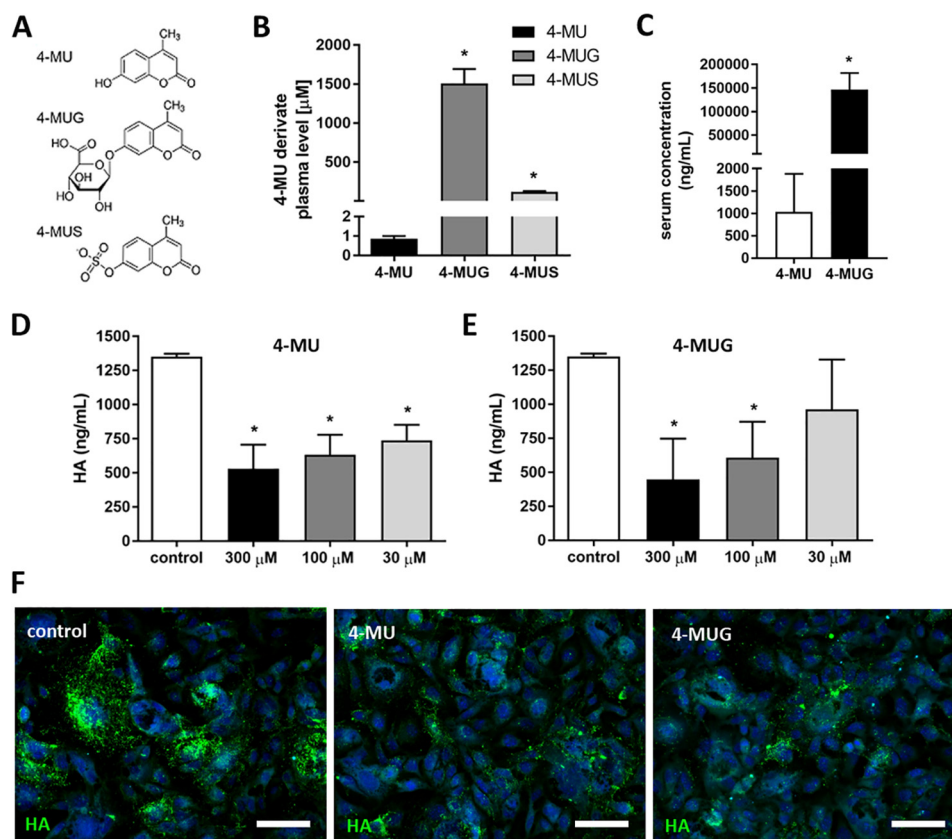
Figure 1. 4-MUG, a metabolite of 4-MU, inhibits HA synthesis. *A*, molecular structures for 4-MU and its primary metabolites, 4-MUG and 4-MUS. *B*, concentrations of 4-MU and its metabolites in plasma of animals fed 4-MU chow for 2 weeks, measured via HPLC. $n = 3$ animals per group. *C*, different concentrations of 4-MU and 4-MUG in the serum of mice fed 4-MU for 2 weeks measured via HPLC. $n = 3$ animals per group. *D* and *E*, HA production by B16F10 cells cultured for 48 h in (*D*) 4-MU or (*E*) 4-MUG. *F*, representative images of HA staining in B16F10 cells cultured in DMSO as control (*left*), 4-MU (*middle*), or 4-MUG (*right*). *Scale bar* = 50 μm. Data represent mean ± S.E.; *, $p < 0.05$ by unpaired *t* test or one way analysis of variance (ANOVA) with Bonferroni post test.

reduces expression of HAS mRNA (33), as well as UDP-glucose pyrophosphorylase and dehydrogenase (34), although the functional contributions of these are unclear. Furthermore, a microarray study revealed that 4-MU alters the cell cycle and the p53 pathways (35). 4-MU treatment prevents many of the inflammatory phenotypes associated with HA, including tumor metastasis, fibrosis progression and autoimmunity (reviewed in Ref. 29). We and others have previously reported that 4-MU promotes the induction of Foxp3$^+$ regulatory T-cells, an important anti-inflammatory cell type, and that 4-MU prevents fibrosis and autoimmunity in multiple animal models of human autoimmune diseases, including multiple sclerosis, T1D, and rheumatoid arthritis (17, 19, 20, 29, 36).

4-MU is a commercially available drug approved for use in humans. Called Hymecromone, it is prescribed in European and Asian countries to prevent biliary spasm (34). This suggests that 4-MU could be repurposed to inhibit HA synthesis in humans. Indeed, 4-MU is under investigation in human clinical trials as a treatment for HA-associated fibrotic liver and autoimmune biliary diseases (identifiers: NCT00225537, NCT02780752).

Unfortunately, 4-MU has poor pharmacokinetics that are thought to limit its use outside the biliary tract. The systemic oral bioavailability of 4-MU is reported to be <3%, mostly because of extensive first pass glucuronidation in the liver and small intestine (37, 38). Any 4-MU that does reach the systemic

circulation is rapidly metabolized with a half-life of 28 min in humans (3 min in mice) and <1% of a given dose is excreted unchanged in the urine (37, 38). Consequently, the median plasma concentration of 4-methylumbelliferyl glucuronide (4-MUG) is more than 3000-fold higher than that of 4-MU in mouse models (29). Analogous findings have been reported in healthy human volunteers (38).

Despite this poor bioavailability and a short half-life, oral administration of 4-MU nonetheless inhibits HA synthesis *in vivo*, suggesting additional factors may potentiate its activity and sustained effect. Given that most of the drug is present in circulation as 4-MUG, we suspected that this metabolite might undergo hydrolysis and reconversion into 4-MU *in vivo*.

Here, we have used MS and 2-photon microscopy to interrogate the tissue-binding patterns of 4-MU in mice and to address specific pharmacologic questions regarding the tissue binding of 4-MU and the hydrolysis of 4-MUG *in vivo*

Results

4-MUG inhibits HA synthesis in vitro

As a result of efficient glucuronidation of 4-MU in the liver and intestines by multiple UGTs, the predominant form present systemically in mice on oral 4-MU chow is 4-MUG (Fig. 1, *A–C*), as has been reported previously (39). The median serum

4-MUG contributes to hyaluronan synthesis inhibition

concentration of 4-MUG was about 150-fold higher than the parent compound 4-MU (Fig. 1C).

Because the activity of metabolites is an important variable in pharmacodynamic determinations, we asked whether the main 4-MU metabolite 4-MUG inhibits HA synthesis. To test this, we used murine melanoma cells (B16F10), a cell line known to produce abundant HA. We observed a concentration-dependent inhibition of HA synthesis in both 4-MU– and 4-MUG– treated B16F10 cells after 48 h of drug exposure (Fig. 1, D and E). Similar findings were seen as well in primary lymphocytes (data not shown). Fluorescent staining of these cells using HA-binding protein, indicated that treatment with 4-MU and 4-MUG both reduced HA (Fig. 1F). Together these results indicate that treatment with either 4-MU or 4-MUG inhibits HA synthesis.

Because there are reports of other glucosaminoglycan (GAG) inhibition by 4-MU at high concentrations, we performed a dimethylmethylene blue (DMMB) assay investigating the specificity of 4-MUG to inhibit HA and its influence on other GAGs. We found that 4-MU and 4-MUG at 300 μM and 100 μM did not significantly inhibit overall GAG production (Fig. S1). 4-MU at 300 μM showed a trend to lower cell-associated GAGs compared with untreated control; however this was not significant (Fig. S1).

Also because of previous investigators' work showing that 4-MU can have toxic effects linked to reactive oxygen species (ROS) production, we performed similar studies using 4-MU and 4-MUG (Fig. S2). As these effects have been most closely researched on leukocytes, similar cells were used here. The human monocyte line U937 cells as well as mouse CD4$^+$ T-cells were treated for 24 h prior to flow cytometry analysis looking at viability, apoptosis (Annexin V), and ROS levels. Although 4-MU shows measurable increases in ROS within the CD4$^+$ T-cells, this is not seen in the U937 cells (Fig. S2, C and F). Furthermore, 4-MUG shows no measurable increases in ROS within either cell population (Fig. S2, C and F). The change of viability measurements under 4-MU and 4-MUG treatment compared with untreated control was less than 1% (Fig. S2, A and D). Overall 4-MUG does not induce reasonable ROS changes that induce either apoptosis (Fig. S2, B and E) or general viability changes.

4-MUG is hydrolyzed into 4-MU within cells

Given the established activity of 4-MU leading to inhibition of HA synthesis, it seemed possible that the bioactivity of 4-MUG could be attributed to its hydrolysis into 4-MU. To examine this, we took advantage of the fact that 4-MU is fluorescent whereas 4-MUG is not (Fig. 2A). In particular, 4-MU has an excitation wavelength of 380 nm and an emission wavelength of 454 nm in water. We added 4-MU or 4-MUG to PBS with 10% FCS and monitored the increase of fluorescence signal using a fluorescence plate reader at intervals up to 72 h (Fig. 2B). As expected, 4-MU had a fluorescent signal at baseline (Fig. 2B). Fluorescence of 4-MUG on the other hand could only be detected starting around 30 h (Fig. 2B). We then added 4-MU and 4-MUG to B16F10 cells; we found that cells treated with 4-MUG became fluorescent after 48–72 h (Fig. 2C). The fluorescence of these cells was lost upon permeabilization (Fig. 2D),

suggesting that most of the fluorescent 4-MU is inside the cell. Together, these data suggest that 4-MUG is taken up by cells and converted back into 4-MU, resulting in its effects on HA synthesis inhibition. However, because the conversion of 4-MUG to 4-MU also takes place in vitro in media alone, it seems likely that extracellular conversion occurs as well.

To test whether 4-MU binding is nonspecific and noncovalent we added 4-MU to B16F10 cells treated with or without hyaluronidase to remove cell surface HA, and we added 4-MU to B16F10 cells washed with a high-salt buffer to remove 4-MU bound to the cell surface by ionic interactions (Fig. S3, A–D). These studies were performed for 1 h and 24 h 4-MU treatment at either 4 °C or 37 °C because enzymatic processes responsible for covalent binding could be expected to require room temperature whereas nonspecific charge–based interactions would not. We observed that more 4-MU was taken up after 24 h compared with the 1 h treatment regardless of temperature (Fig. S3, A–D). Furthermore, we saw no difference in 4-MU signal under the different treatments (Fig. S3, A–D). We conclude that 4-MU does not directly bind to HA and the cell surface.

4-MU is taken up by lymphocytes

We further asked whether 4-MU and 4-MUG are taken up by circulating cells and tissues in vivo. To this end, we again took advantage of the fluorescence of 4-MU to use as a biomarker of 4-MU uptake. We first assessed 4-MU signal on cells isolated from spleen tissue and blood of mice that had been on oral 4-MU treatment for at least 14 days. Using the Pacific Blue channel, we could readily observe 4-MU signal on splenocytes (Fig. S4A) and circulating leukocytes (Fig. S4B) from mice that were treated with 4-MU, indicating that 4-MU is taken up by cells within lymphatic tissues in vivo as well as binding to the extracellular matrix.

Next, we examined the uptake of 4-MU by different leukocyte subsets (Fig. 3). To this end, we fed mice 4-MU and examined 4-MU signal on blood leukocytes from representative animals at intervals of 0, 2, 7, and 14 days after the initiation of 4-MU treatment (Fig. 3). We stained for cell surface markers to examine 4-MU uptake by multiple cell types, including CD4$^+$ T-cells (CD3$^+$CD4$^+$), CD8$^+$ T-cells (CD3$^+$CD8$^+$), B-cells (I-A/I-E$^+$B220$^+$), dendritic cells (I-A/I-E$^-$CD11c$^+$), macrophages (I-A/I-E$^+$CD11c$^-$), neutrophils (Ly6G/C$^+$CD14$^+$), and monocytes (Ly6G/C$^-$CD14$^+$). A representative FACS gating scheme is displayed in Fig. S5.

The fluorescent 4-MU signal was not seen in mice treated for 48 h, but started to be visible after 1 week of treatment (Fig. 3). This is consistent with our previous report that 1–2 weeks of oral 4-MU treatment was necessary for effects on hyaluronan synthesis to become apparent (40). We find that by day 7 after 4-MU treatment 4-MU signal was marginally visible in all of these cell populations and by day 14 all signals were decisively increased to varying extent (Fig. 3). These data show that multiple leukocyte populations take up 4-MU and that a time period of between 1 and 2 weeks is required for this to occur. Together, these data indicate that 4-MU is taken up by resident cells.
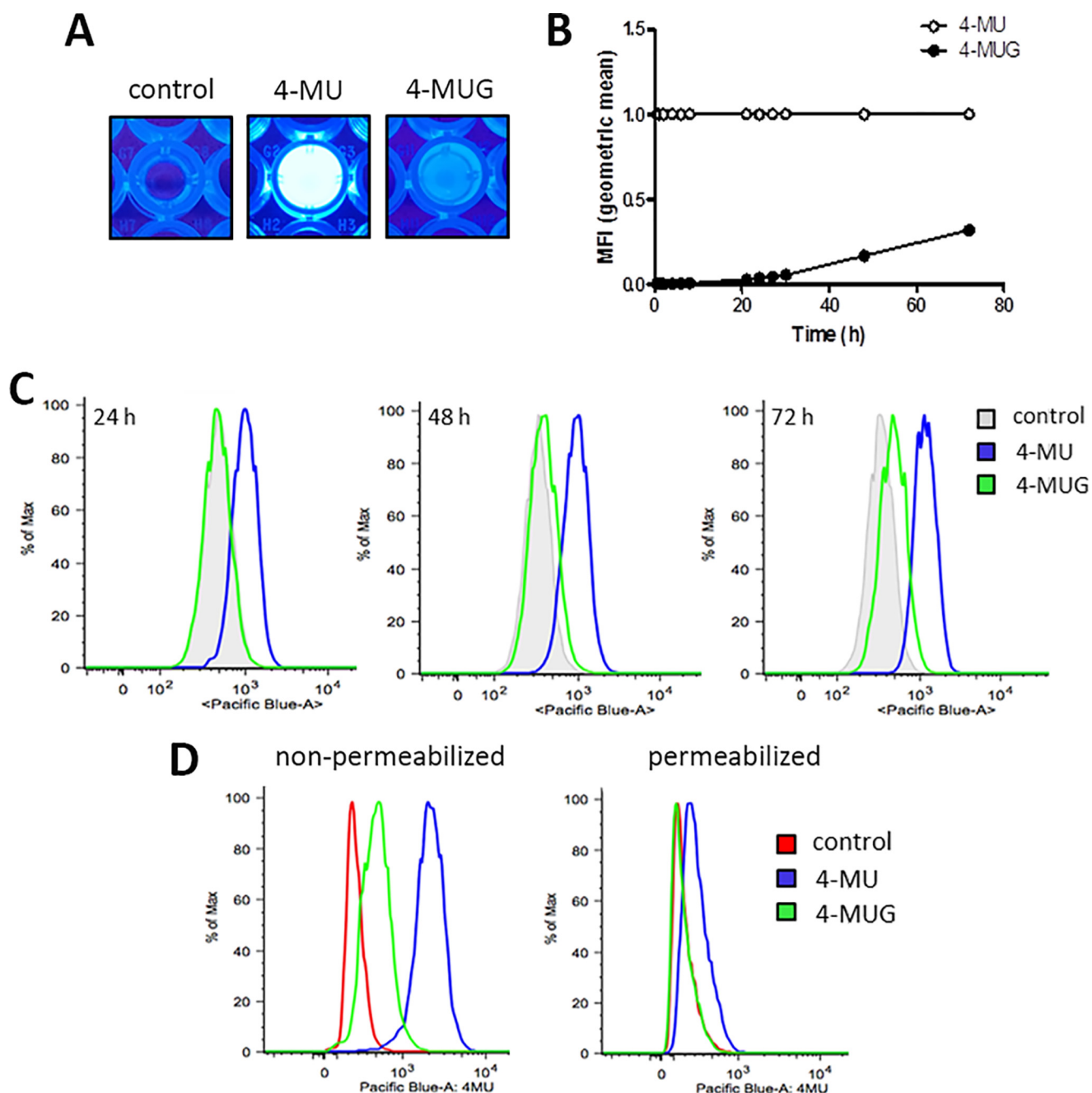
Figure 2. 4-MUG is converted into 4-MU *in vitro*. *A*, fluorescence visualization in wells of a 96-well plate which was filled with 200 μl PBS and 10% FCS. In some wells 4-MU (*middle*) and 4-MUG (*right*) were added; control wells remained untreated (*left*). *B*, 4-MU and 4-MUG were separately added to DMEM and their fluorescent signal over time was measured as mean fluorescent intensity (*MFI*). Fluorescent values of 4-MUG were normalized to the 4-MU fluorescence. *C*, fluorescence of 4-MU and 4-MUG from B16F10 cells incubated for 24, 48, or 72 h with 4-MU and 4-MUG examined using flow cytometry. *D*, fluorescence of 4-MU and 4-MUG signal from 4-MU– and 4-MUG–treated B16F10 cells pre- and post-permeabilization was examined by flow cytometry.

4-MU is bound to tissue extracellular matrix structures within lymph nodes in vivo

To investigate 4-MU tissue binding *in vivo*, we examined 4-MU fluorescence in mice using intravital 2-photon imaging, a tool that allows imaging fluorescent signals deep within tissues. We first examined 4-MU binding within lymph nodes, structures with well-defined architecture, including capsules, germinal centers, the sites of B-cell development, and interfollicular regions, the sites of T-cell development (Fig. 4*A*). The extracellular matrix polymer HA, in *brown*, is present at all sites of the lymph node (Fig. 4*B*).

We find that 4-MU is bound to reticular fibers within the lymph node, structures which are known to contain collagen III (Fig. 4, *C* and *D*), but we find that mostly 4-MU did not colocalize with collagen (Fig. 4, *C* and *D*). 4-MU deposition along reticular fibers tended to be most dense within areas rich in CD11c$^+$ dendritic cells and less dense within T-cell zones (Fig. 4*E*). The 4-MU signal was minimal in lymph nodes of control mice not on the drug (Fig. 4*F*), indicating a low level of background noise. Collagenase treatment removed the collagen fluorescent signal but also digested the lymph node tissue (data not shown).

⧉ASBMB

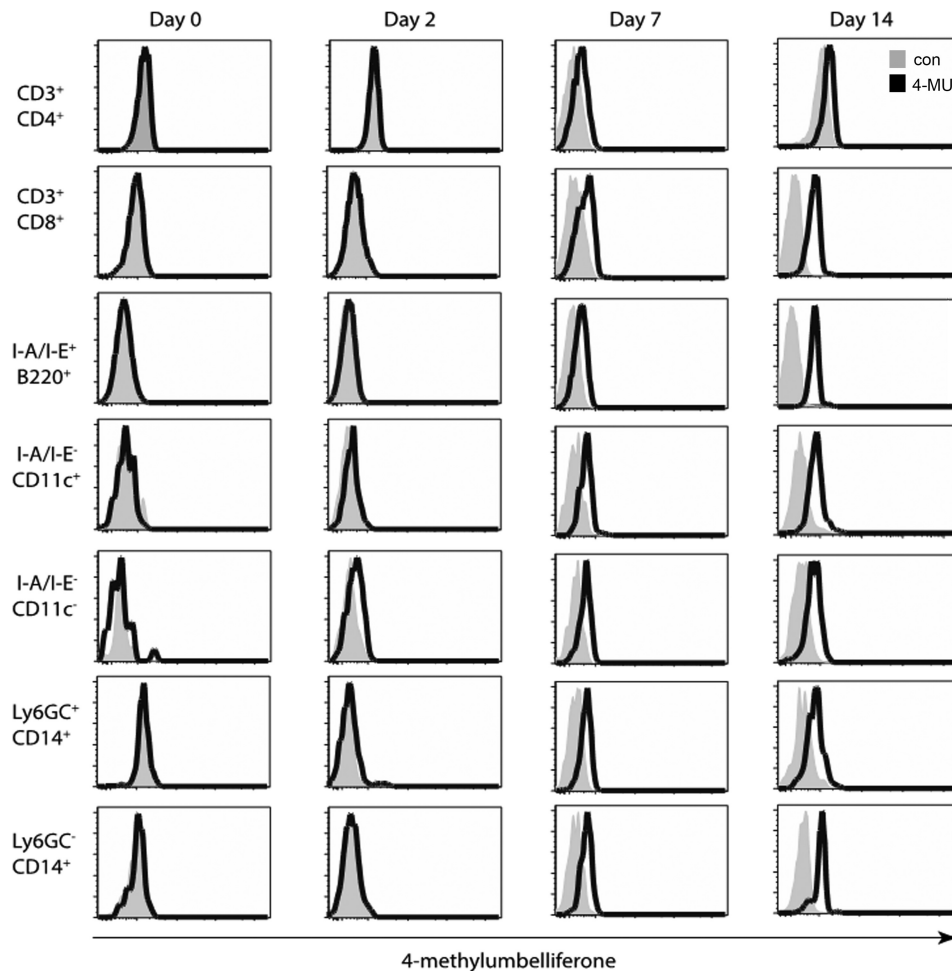*J. Biol. Chem.* (2019) 294(19) 7864–7877   **7867**

Figure 3. 4-MU is taken up by leukocytes *in vivo.* Mice were treated with 4-MU. Signal on different cell subsets in the blood was analyzed by flow cytometry, as measured in the Pacific Blue channel, before and 2, 7, and 14 days after start of treatment. Bold histograms depict signal in 4-MU treated mice, tinted histograms depict background Pacific Blue signal in untreated mice.
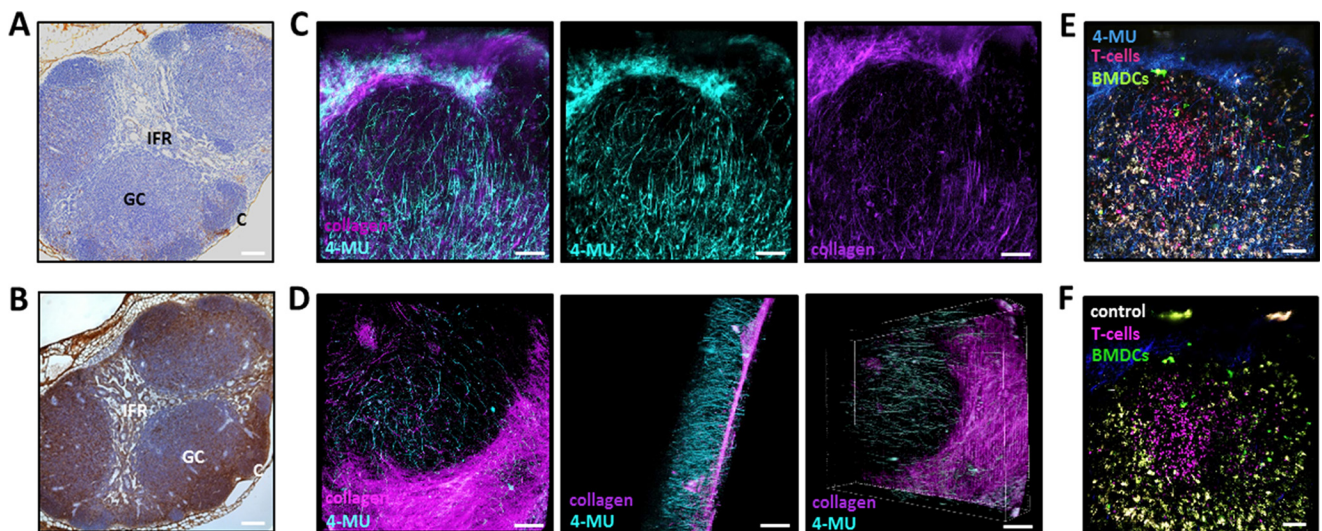
Figure 4. 4-MU tissue binding can be visualized using 2-photon microscopy. *A* and *B*, representative images of mouse lymph nodes stained for H&E (*A*) and HA (*B*). C, capsules; GC, germinal centers; IFR, interfollicular regions. *Scale bar* = 150 μm. *C* and *D*, mice were treated with 4-MU and the tissue distribution could be detected and visualized in the lymph node. Representative images showing 4-MU signal in *blue/green* and collagen signal in *purple*. *Scale bar* = 100 μm. *E* and *F*, representative images of mouse lymph nodes from 4-MU treated (*E*) and untreated control (*F*) mice, showing signal from 4-MU, T-cells, and BMDCs. *Scale bar* = 100 μm.

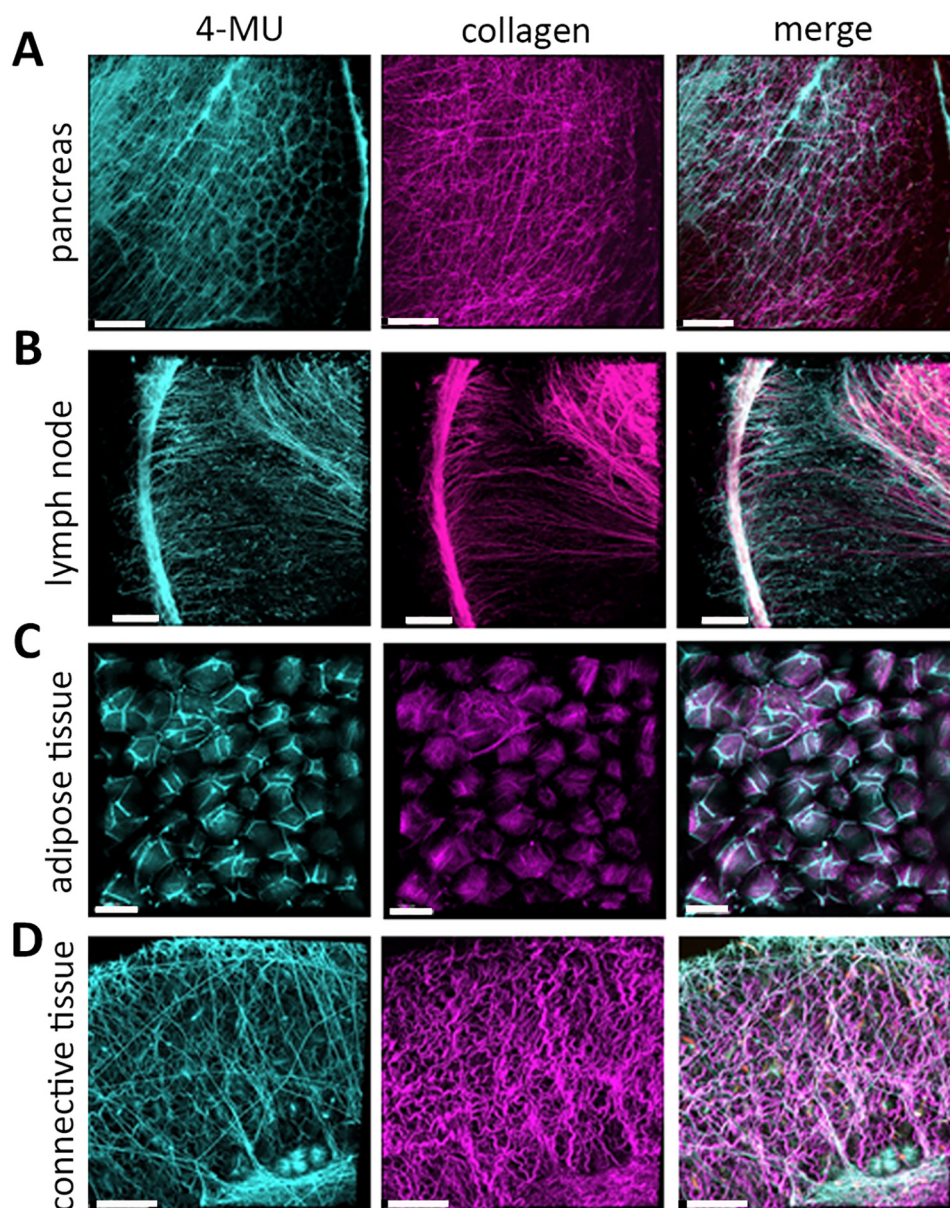**Figure 5. 4-MU fluorescence can be used to show tissue distribution via 2-photon imaging.** Mice were treated with 4-MU and the tissue distribution could be detected and visualized in multiple organs. *A–D*, representative images showing 4-MU and collagen signals in pancreas (*A*), lymph node (*B*), adipose tissue (*C*), and connective tissue (*D*). In each of those tissues 4-MU has a specific distribution as shown at 810 nm wavelength (shown in *light green*). Collagen was visualized at 920 nm (shown in *purple*), the 4-MU and collagen channel were merged for better structural orientation in the tissue. *Scale bar* = 100 μm.

4-MU binds to extracellular matrix within multiple tissue types

Further intravital 2-photon imaging experiments in mice revealed that 4-MU signal is seen in the pancreas, lymph nodes, adipose tissue, and connective tissue from mice treated with 4-MU for 2 weeks (Fig. 5, *A–D*; Fig. 6A). We also find that mice treated with 4-MUG for 2 weeks likewise showed a 4-MU signal (Fig. 6B) whereas mice treated with 4-MU for 3 or 7 days had no signal (data not shown). The 4-MU signal is visible at an excitation wavelength of 810 nm, which is absent in mice that received control chow (Fig. 6C).

4-MU binding is most prominent within structures associated with the extracellular matrix. Within lymph nodes, 4-MU is abundant within the tissue capsules and linear, reticular-fiber like structures (Fig. 5B, *left image*). Many of these sites overlap

somewhat with the distribution of collagen (Fig. 5B, *right image*). Within muscle and adipose tissue 4-MU binding likewise overlaps with the distribution of collagen but not with blood vessels (Fig. S6, *A* and *B*). Furthermore, hyaluronidase treatment of muscle tissue from a 4-MU–treated mouse demonstrated a reduction of 4-MU signal (Fig. 6D). This could have been caused by tissue degradation because of the hyaluronidase treatment protocol, because the collagen in the hyaluronidase-digested tissue looked altered as well (Fig. 6D).

In vivo administration of 4-MU or 4-MUG leads to the same serum ratio of 4-MU to 4-MUG

To confirm our 2-photon imaging results, that 4-MU or 4-MUG were present in tissues, and to better characterize the
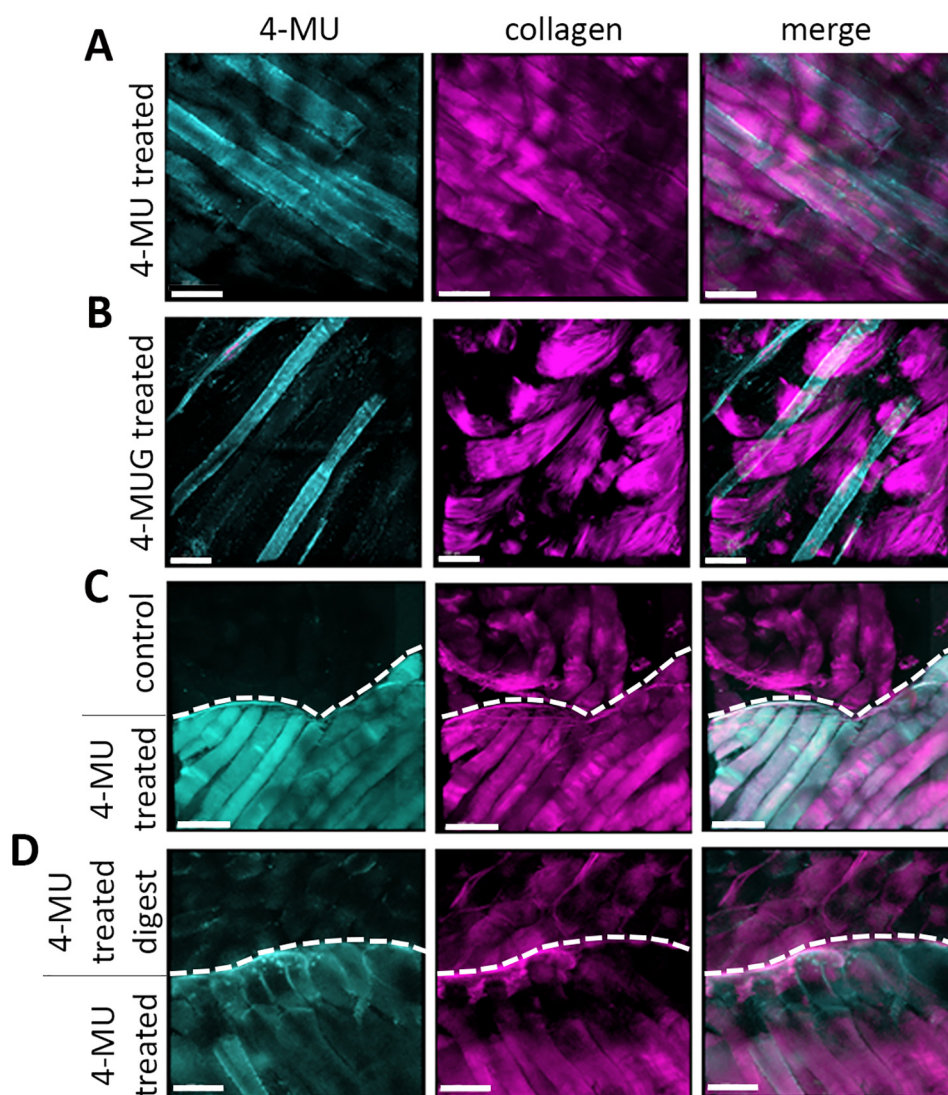
Figure 6. 4-MUG fluorescence can be detected in tissues via 2-photon imaging. *A* and *B*, representative 2-photon images of muscle tissue from 4-MU–treated mice (*A*) and 4-MUG–treated mice (*B*) show a specific signal in the 4-MU channel at a wavelength of 810 nm. *C*, representative 2-photon images of muscle tissue from untreated control mice (*upper part*) and 4-MU treated mice (*lower part*). *D*, representative 2-photon images of muscle tissue from 4-MU treated mice, where the muscle tissue from one mouse (*upper part*) was hyaluronidase digested. Untreated muscle tissue from a 4-MU treated mouse (*lower part*) serves as control. Upper and lower parts are indicated via a *dashed line* drawn in the picture. In each of those tissues 4-MU has a specific distribution as shown at 810 nm wavelength. Collagen was visualized at 920 nm, the 4-MU and collagen channel were merged for better structural orientation in the tissue. *Scale bar* = 100 μm.

interconversion between 4-MUG and 4-MU, we performed LC-MS (LC-MS/MS) (Fig. S7) on serum, muscle, liver, fat, and pancreatic tissues from untreated mice or mice treated with either 4-MU or 4-MUG (Fig. 7).

We found that the resulting ratio between 4-MU and 4-MUG present in serum arrived at a molar ratio of 1:72.5 irrespective of which drug was administered (Fig. 7*B*), indicating the two compounds exist in equilibrium together. Although the same amount of each drug was bioavailable as indicated by the same ratios, the level of 4-MU and 4-MUG were lower in the 4-MUG–treated mice compared with the 4-MU–treated mice (Fig. 7*A*), suggesting that 4-MUG may be absorbed with greater efficiency. In 4-MU–treated animals, higher levels of 4-MU were seen in serum than in pancreatic tissue (1005 ng/ml *versus* 64.8 ng/ml) (Fig. 7, *A* and *C*). However, substantially higher levels of 4-MU were seen in pancreatic tissue than in serum for

mice fed 4-MUG (10,200 ng/ml *versus* 2.5 ng/ml) (Fig. 7, *A* and *C*). The ratio of 4-MU:4-MUG in serum (1:73 for 4-MU treatment and 1:72 for 4-MUG treatment) (Fig. 7*B*) was far less than the ratio of 4-MU:4-MUG in pancreas (1:0.27 for 4-MU treatment and 1:0.45 for 4-MUG treatment) (Fig. 7*D*), suggesting that 4-MU is more efficiently bound within tissues than 4-MUG. We furthermore investigated the 4-MU and 4-MUG concentrations in fat (Fig. 7, *E* and *F*), liver (Fig. 7, *G* and *H*), and muscle (Fig. 7, *I* and *J*). We observed a similar 4-MU:4-MUG ratio in fat and muscle; here the 4-MU–treated animals had a significantly higher amount of 4-MUG compared with the 4-MUG treatment (Fig. 7, *F* and *J*). Interestingly, the liver similarly to serum showed an equilibrium between 4-MU and 4-MUG no matter what the treatment was (Fig. 7, *G* and *H*). The liver has a high concentration of 4-MU compared with 4-MUG independent of treatment (Fig. 7*H*). Together,
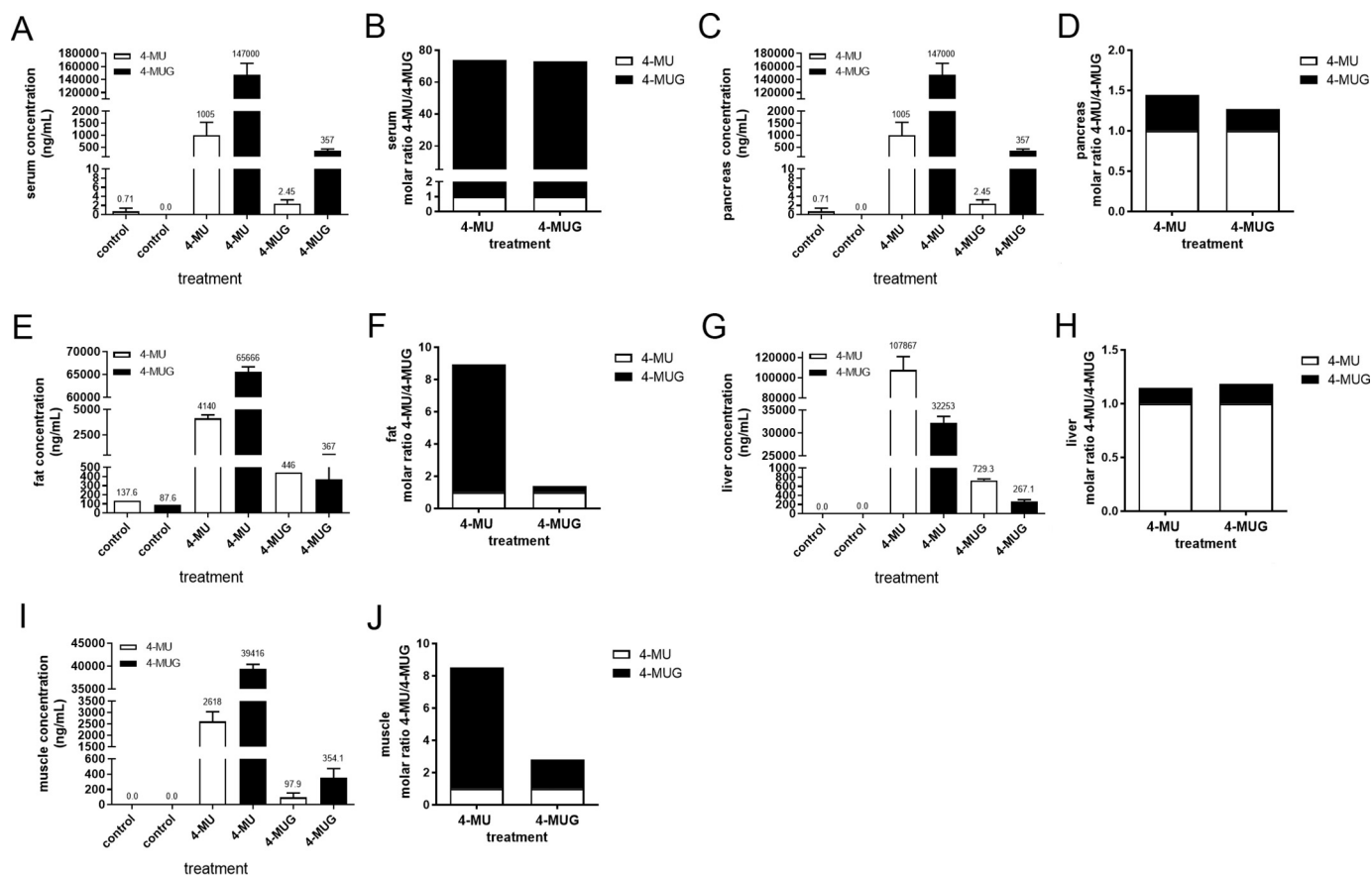
Figure 7. 4-MU and 4-MUG concentrations in serum and organs from 4-MU and 4-MUG treated mice. *A, C, E, G*, and *I*, 4-MU and 4-MUG concentrations were analyzed in the serum (*A*), pancreas (*C*), fat (*E*), liver (*G*), and muscle (*I*) from untreated control mice and 4-MU– and 4-MUG–treated mice using LC-MS/MS. *n* = 3–5 mice per group. *B, D, F, H*, and *J*, calculated molar ratio of 4-MU and 4-MUG from serum (*B*), pancreas (*D*), fat (*F*), liver (*H*), and muscle (*J*) in the different treatment groups. Data represent mean ± S.E.

these data indicate that 4-MUG is converted into 4-MU *in vivo*, that 4-MU is taken up by a range of tissues and cell types *in vivo*, and that tissue structures serve as a reservoir for 4-MU.

4-MUG treatment slightly reduces HA production, HAS1–3 mRNA expression, and UDPGA concentration in vivo

Because we have shown that 4-MU and 4-MUG reduced HA content *in vitro*, we wanted to know if 4-MUG reduces HA *in vivo* as well. To test this, we treated mice with 4-MU and 4-MUG and assessed the HA content of different mouse tissues via HA ELISA. We found that in the pancreas, muscle, fat, and liver no significant decrease of HA concentration of either treatment could be detected (Fig. S8, *A–D*). A slight reduction of HA was seen in the different tissues regardless of treatment compared with untreated control (Fig. S8, *A–D*). This rather small effect could be explained by the fact that we used nondiseased mice for this study with overall low HA concentrations.

Because it is known that 4-MU also inhibits HA production by reduction of HAS mRNA expression, we examined the effect of 4-MU and 4-MUG on HAS1–3 gene expression. We treated B16F10 cells and mice with 4-MU and 4-MUG and performed RT-qPCR analysis (Fig. S9). The B16F10 cells after 4-MU treatment revealed a concentration-dependent, slight, nonsignificant decrease in HAS1–3 expression,

whereas 4-MUG treatment showed no difference in HAS1–3 expression (Fig. S9, *A, E,* and *I*). We further examined muscle, pancreas, and liver from 4-MU– and 4-MUG–treated mice and found that 4-MU significantly reduces the HAS1 expression in muscle and liver (Fig. S9, *B–D*). A general trend of expression reduction for HAS1–3 could be observed under 4-MU treatment (Fig. S9). 4-MUG significantly reduced HAS1 expression in the muscle (Fig. S9*B*); all other tissues and HAS isoforms did not seem to be majorly affected by 4-MUG treatment (Fig. S9).

We next tested the originally described mechanism of 4-MU's HA inhibition, the depletion of the HA precursor UDP-glucuronic acid (UDPGA). We measured the UDPGA concentration in different tissues from 4-MU– and 4-MUG–treated cells and animals (Fig. S10). We observed that 4-MU at a high concentration significantly reduced the UDPGA concentration in the cell pellet as well as in the mouse pancreas, muscle, and spleen (Fig. S10, *B, D, E,* and *H*). In the cell supernatant and the other tissues 4-MU showed a trend toward UDPGA down-regulation but this was not significant (Fig. S10, *A, C, F,* and *G*). 4-MUG on the other hand had no effect on the UDPGA concentration (Fig. S10, *A–H*). Together these results indicate that compared with 4-MU, 4-MUG might have a somewhat different mechanism of action profile regarding HA inhibition.
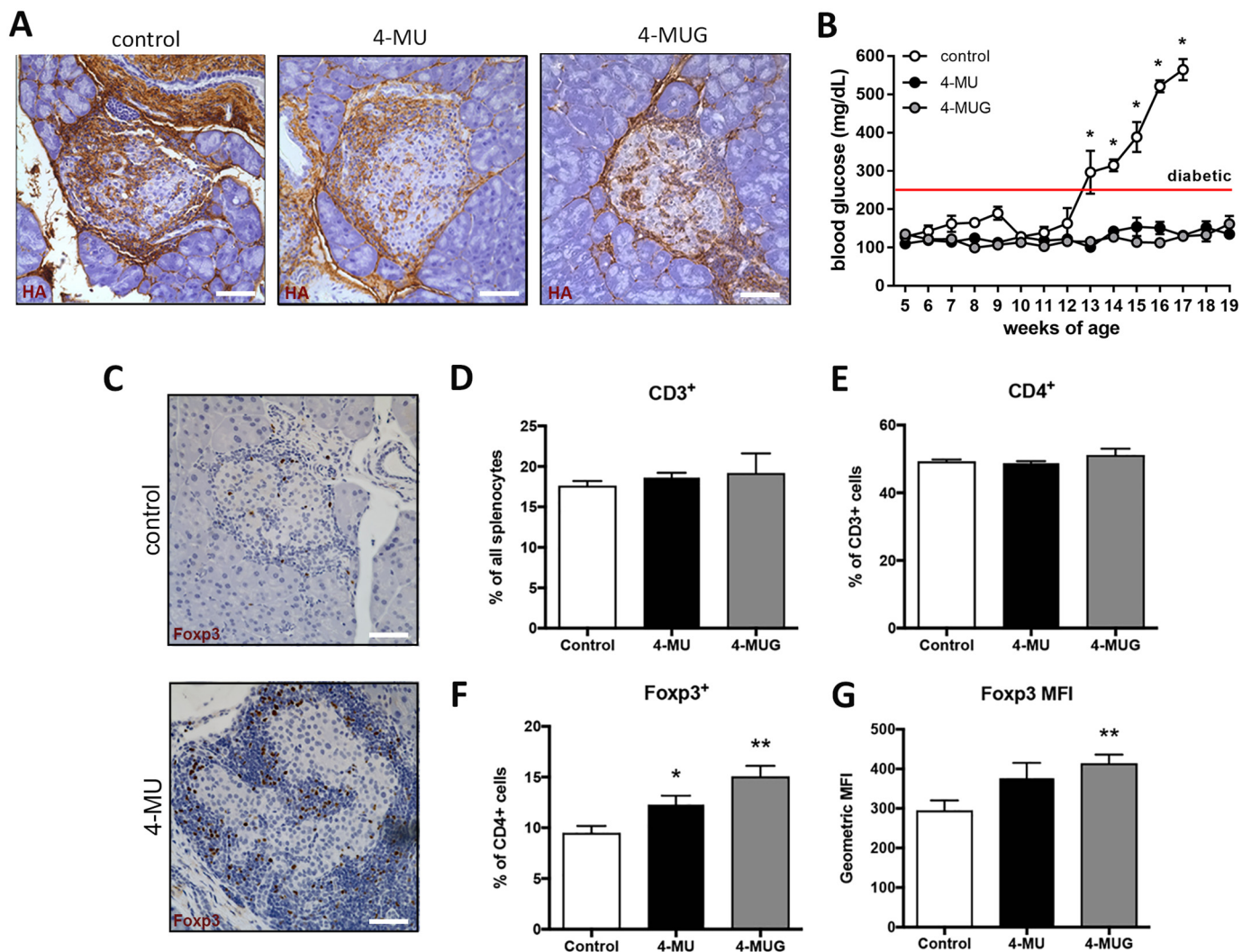
Figure 8. 4-MU and 4-MUG treatment prevents progression in autoimmune diabetes and increases Treg numbers. *A*, representative HA staining of pancreatic tissue from untreated DORmO mice (control), DORmO mice fed 4-MU, and DORmO mice fed 4-MUG, at 12 weeks of age. *B*, blood glucose of untreated DORmO mice, and DORmO mice fed 4-MU and 4-MUG, beginning at 5 weeks of age, and maintained on 4-MU and 4-MUG for 15 weeks. $n = 5$–10 mice per group. Data represent mean $\pm$ S.E. *C*, representative FoxP3 staining (*brown*) of pancreatic islet tissue from untreated (control) and 4-MU treated DORmO mice. Original magnification, $\times$40. *D–G*, numbers of CD3$^+$ cells, CD4$^+$ among CD3$^+$ cells, and Foxp3$^+$ among CD3$^+$/CD4$^+$ cells, in splenocytes isolated from mice that were treated with 4-MU (0.5 mg i.p.) or 4-MUG (1 mg i.p.) daily for 14 days, as analyzed by flow cytometry. *Scale bar = 20 μm. *, $p < 0.05$; **, $p < 0.01$ by unpaired *t* test with Welch's correction. Data represent mean $\pm$ S.E.*

4-MUG inhibits diabetes progression and induces Foxp3 expression in T1D mice

To assess whether 4-MUG administration inhibited HA synthesis *in vivo*, as we have previously shown for 4-MU (17), we administered this drug to our animal model of T1D, the DO11.10xRIPmOVA (DORmO) mouse. DORmO mice carry a T-cell receptor transgene specific for OVA (emulating autoreactive CD4$^+$ T-cells), while simultaneously expressing OVA in conjunction with the insulin gene promoter on pancreatic beta cells (emulating the autoantigen). Representative histologic images of DORmO pancreatic islets show that CD3 T-cells, in brown, are surrounding and invading the pancreatic islets of untreated mice, whereas the T-cell staining in the 4-MU treated mice is mainly surrounding the islet, the islet itself is mostly intact (Fig. S11A). Staining the DORmO islets for HA, in brown, we could demonstrate a decrease of HA accumulation after 4-MU and 4-MUG treatment compared with untreated DORmO mice (Fig. 8A). Consistent with this, 4-MUG treatment delayed the onset of T1D as measured by blood glucose over time compared with untreated DORmO mice (Fig. 8B). In line with the normo-glycemic blood glucose, insulin positive cells were preserved in the pancreatic islets under 4-MU treatment (Fig. S11B). Further, we observed an increase of Foxp3 regulatory T-cells (Tregs) in the pancreatic islets of the nondiabetic 4-MU treated DORmO mice (Fig. 8C) and we found that both 4-MU and 4-MUG treatment of WT control mice resulted in an increase of Tregs, as well as an increase in their expression of Foxp3$^+$ (Fig. 8, *F and G*), CD4+ and CD3+ T-cell numbers were not affected by either treatment (Fig. 8, *D and E*). A representative FACS gating scheme is shown in Fig. S12. These observations are consistent with recent reports by our group and others that 4-MU induces Foxp3$^+$ Treg in multiple animal models.

Discussion

We report that 4-MUG contributes to the bioactivity of 4-MU both *in vitro* and *in vivo* via conversion into 4-MU. Indeed, 4-MU and 4-MUG were almost equally effective over a range of concentrations at inhibiting HA synthesis by cancer cell lines *in vitro*. Both were likewise equally effective in treating autoimmunity in a mouse model of T1D.

These data suggest that our understanding of the pharmacodynamics of 4-MU needs to be revised to reflect the presence of 4-MUG. In our published animal studies, 4-MUG was present at concentrations 300-fold higher than those seen for the parent molecule, 4-MU. Consistent with this, in humans 4-MUG accounts for over 90% of 4-MU metabolism (37, 38).

It is possible to administer 4-MUG to achieve the same effects as administering 4-MU both *in vitro* and *in vivo*. Our *in vivo* experiments in the DORmO mouse model of T1D showed that there is no visible difference in HA reduction in the pancreatic islets or reduction of blood glucose between 4-MU and 4-MUG treatment; both are sufficient to stop diabetes progression. This implies that 4-MUG provides an alternative therapeutic option in the treatment of autoimmune diseases. Indeed, 4-MUG has some advantages over 4-MU as a drug as 4-MUG is water-soluble and can be administered in the drinking water. It remains possible that other metabolites of 4-MU likewise are bioactive. However, these metabolites are present at such low levels (<1% of drug level) (40) that these are unlikely to contribute substantially to overall effects on HA and therefore were not tested.

We also report that tissue binding of 4-MU can be observed *in vivo* using 2-photon microscopy. In particular, 4-MU binds to collagen-rich structures within the tissue matrix and is also taken up by a variety of cells within the lymph nodes, pancreas, fat, liver, and muscle. We conclude that 2-photon intravital microscopy could be used as a novel platform for interrogating tissue binding of fluorescent drugs and that it may be possible to combine this approach with other readouts of compound activity or tissue localization.

The fluorescent signal we observed via FACS on cells was substantially diminished upon permeabilization, suggesting that at least some of the drug is present intracellularly. In tissues, the fluorescent signal could be lost by treatment with collagenase or hyaluronidase, indicating that 4-MU may be bound to these molecules. These findings were corroborated by LC-MS/MS, indicating that tissues indeed contain 4-MU as well 4-MUG. It is possible that the drug is incorporated into growing HA polymers but this seems unlikely, given the known mechanisms of HA synthesis. Studies revealed that changing the availability of UDP-GlcUA led to a change in HA production but had no effect on other GAGs (35). This is because UDP-sugar concentrations can be altered in the cytosol where HA is produced, but not inside the Golgi, where the sulfated GAGs are synthesized (41). High-affinity transporters for sugar nucleotides are located in the Golgi membranes (42), which maintain high concentrations of UDP-sugars inside the Golgi, even if the cytosolic availability is low. Only HA is affected by UDP-sugar availability, as HASes use sugar precursors directly from the cytosolic pool. HA is normally synthesized by three HA synthases which use UDP-sugars of GlcNAc and glucuronic acid as precursors for HA. In the presence of 4-MU, HA synthesis is inhibited by lowering the supply of UDP-glucuronic acid. 4-MU is an excellent substrate for UGT, and as a result UGT consumes huge amounts of UDP-glucuronic acid, transferring the glucuronic acid onto 4-MU, thereby depleting the cellular precursor pool which leads to inhibition of HA synthesis. Therefore it is unlikely that 4-MU gets incorporated into HA during its synthesis. Interestingly, 4-MUG neither reduces HAS mRNA expression nor the HA precursor UDPGA, suggesting a different mechanism of action.

Together, these studies indicate that 4-MU is more bioavailable than was previously believed because of the contributions of its metabolite 4-MUG. This insight alters the experimental and therapeutic picture for 4-MU and may facilitate the development of potential therapeutic strategies targeting HA synthesis in cancer, autoimmunity, and other indications (29, 43).

Experimental procedures

Mice

All animals were bred and maintained under specific pathogen-free conditions, with free access to food and water, in the animal facilities at Stanford University Medical School (Stanford, CA). B6.db/db LeptR$^{-/-}$ mice were purchased from The Jackson Laboratory as well as DO11.10 transgenic mice. The DO11.10 mice were bred with Balb/c mice expressing RIP-mOva (available at the Benaroya Research Institute) to generate the DORmO double-transgenic mice. In addition, C57Bl/6J mice were bred in-house at Stanford University School of Medicine.

Mice diabetes monitoring

Beginning at 4 weeks of age, mice were weighed weekly as well as bled via the tail vein for the determination of their blood glucose level using a Contour blood glucose meter and blood glucose monitoring strips (Bayer Healthcare). When two consecutive blood glucose readings of 250 mg/dl were recorded, animals were considered diabetic. When two consecutive blood glucose readings of 300 mg/dl were recorded, animals were euthanized.

4-MU and 4-MUG treatment

The 4-MU (Alfa Aesar) was pressed into the mouse chow by TestDiet® and irradiated before shipment, as described previously (31). We previously determined that this chow formulation delivers 250 mg/mouse/day, yielding a serum drug concentration of 640.3 ± 17.2 nmol/liter in mice, as measured by HPLC-MS. 4-MUG (ChemImpex) was distributed in the drinking water at a concentration of 2 mg/ml, delivering 10 mg/mouse/day, yielding a serum drug concentration of 357.1 ± 72.6 ng/ml in mice, as measured by LC-MS/MS. Mice were initiated on 4-MU and 4-MUG at 5, 8, or 12 weeks of age, unless otherwise noted, and were maintained on this diet until they were euthanized, unless otherwise noted. For analysis of Foxp3$^+$ regulatory T-cell numbers in naïve mice, mice were treated daily with 0.5 mg of 4-MU or 1.0 mg 4-MUG in 200 μl 0.08% carboxymethylcellulose in saline by i.p. injection.

SASBMB

J. Biol. Chem. (2019) 294(19) 7864–7877 **7873**

4-MUG contributes to hyaluronan synthesis inhibition

Cell culture

B16F10 cells were cultured in DMEM and were treated with different concentrations of 4-MU and 4-MUG (30, 100, 300 μM) for 1, 24, and 48 h. For certain experiments, cells were treated with hyaluronidase or a 100 mM NaCl salt wash for at 4 °C or 37 °C after 4-MU treatment prior to analyzing the 4-MU signal via flow cytometry. Cultured cells were lysed and analyzed for HA concentration determination using a HA ELISA and mRNA expression of HAS1–3. HA staining in B16F10 cells placed in 96-well plates were imaged (*green*) using fluorescence microscopy. To measure 4-MU florescence intensity in B16F10 cells treated with 4-MU and 4-MUG, B16F10 cells were trypsinized and 4-MU fluorescence associated with the cells was analyzed by flow cytometry in the Pacific Blue channel using a BD LSRII flow cytometer. For permeabilization, after trypsinization, cells were incubated in methanol at −20 °C for 20 min and washed once before flow cytometric analysis.

Leukocyte 4-MU uptake assessments

C57Bl/6J mice were treated with 4-MU, and leukocytes from representative animals were isolated from the blood at baseline (before 4-MU treatment) and at intervals of 2, 7, and 14 days after the initiation of chow. Peripheral venous blood was collected in heparin-coated tubes after cutting the tail veins of mice on 4-MU or control chow. After isolation, blood samples were centrifuged ($1000 \times g$, 4 °C) for 30 min. The serum supernatant was extracted to detect HA levels using a modified HA ELISA as described previously (17). To detect fluorescence emitted by 4-MU using flow cytometry on specific leukocyte subsets, peripheral blood red blood cells were lysed using ammonium-chloride-potassium buffer, and leukocytes were stained with the following fluorochrome-conjugated antibodies: BV650-CD3 (17-A2), BV785-CD4 (RM4–5), APC-CD11c (N418), PE-CD14 (Sa2–8), PE-Cy7-Ly-6G/C (RB6-8C5), PE-Cy5.5-B220 (RA3–6B2), and FITC-I-A/I-E (MHC class II) (M5/114.15.2) from BD Biosciences. Cells were stained for 30 min at room temperature following blockage of Fc receptors (CD16/32, 2.4G2) for 10 min. Samples were washed once with 1 ml FACS buffer (PBS containing 2% FBS and 1 mM EDTA) and fixed with 1.6% paraformaldehyde. Samples were run on a LSRII flow cytometer (Beckon Dickinson) at the Stanford Shared FACS Facility and data were analyzed using FlowJo software (TreeStar).

LC-MS/MS analysis of UDPGA, 4-MU, and 4-MUG concentrations in cells and mouse tissues

UDPGA, 4-MU, and 4-MUG concentrations were measured via MS. UDP-glucuronic acid-3C1, 5N2 Tri-ammonium salt was used as the internal standard (IS) for UDPGA, 4-methyl-umbelliferone-13C4 (Toronto Research Chemicals, Ontario, Canada) was used as the IS for 4-MU, and 7-hydroxycoumarin β-D-glucuronide (Toronto Research Chemicals, Ontario, Canada) as the IS for 4-MUG. The neat stock solutions of UDPGA, 4-MU, and 4-MUG were mixed and diluted in 50% methanol to prepare the spiking solutions ranging from 1 ng/ml to 5000 ng/ml for each compound.

Tissue samples were weighed and 1 volume of stainless steel bullet blender beads (Next Advance) and 3 volumes of Milli-Q

water were added. Tissues were homogenized by a bullet blender (Next Advance) at 4 °C according to manufacturer's instruction. For calibration standards, 25 μl of blank serum or tissue homogenate was mixed with 25 μl of the spiking solutions. For samples to be tested, 25 μl of serum or tissue homogenate was mixed with 25 μl of 50% methanol to make up the volume. 25 μl of a mixture of the two IS (1000 ng/ml each in 50% methanol) was then added. After vortexing all standards and samples, 150 μl of methanol/acetonitrile 20:80 (v/v) was added to the mixture and the sample was further vortexed vigorously for 1 min followed by centrifugation at 3000 rpm for 10 min. 100 μl of the supernatant was taken and diluted with 200 μl of Milli-Q water.

The LC-MS/MS system consists of an AB Sciex QTRAP 4000 mass spectrometer linked to a Shimadzu UFLC system. Mobile phase A is HPLC grade water. Mobile phase B is HPLC grade acetonitrile. LC separation was carried out on a Phenomenex Luna PFP(2) column (3 μm, 150 $\times$ 2 mm) with isocratic elution using 45% mobile phase B and a flow rate of 0.4 ml/min at room temperature. The analysis time was 2.5 min. 10 μl of the extracted sample was injected. The mass spectrometer was operated in the negative mode with the following multiple-reaction monitoring (MRM) transitions: m/z 174.7→132.9 for 4-MU, m/z 178.7→134.9 for 4-MU-13C4 (IS), m/z 350.8→174.9 for 4-MUG, and m/z 336.9→160.9 for 7-hydroxy coumarin β-D-glucuronide (IS). Data acquisition and analysis were performed using the Analyst 1.6.1 software (AB Sciex).

Measurement of HA levels

Cell and tissue samples were thawed and assayed for HA levels using a modified HA ELISA as described previously (17). Each sample was analyzed in triplicate with a mean value obtained per sample. For cell normalization, LI-COR Biosciences CellTag 700 Stain was used according to the manufacturer's protocol.

Dimethylmethylene blue (DMMB) assay

A total of 1×10^7 B16F10 cells per T75 were treated for 24 h with 4-MU and 4-MUG at 300 and 100 μM, supernatant was removed, cell layer was scraped and centrifuged. The resulting cell pellet was digested with 20 μg/ml proteinase K in TBS, 0.5% Triton X-100. Samples were digested at 56 °C for 8 h, following a heat inactivation for 20 min at 100 °C. Insoluble debris was removed by centrifugation at $17,000 \times g$. The GAG content was precipitated by addition of 3 volumes of ethanol overnight at 4 °C, the pellets were collected by centrifugation, and pellets were resuspended in 50 μl of water. 20 μl of the clarified suspension was used for the DMMB assay. The assay was performed as described previously (44).

Tissue processing and imaging

Tissues for histochemistry were extracted from the animals and immediately transferred into 10% neutral buffered formalin. The tissue was processed to paraffin on a Leica ASP300 Tissue Processor (Leica Microsystems Inc.). Then 5-μm-thick sections were cut on a Leica RM2255 microtome (Leica Microsystems Inc.). All staining steps were performed on a Leica BOND MAX automated immune histochemistry stainer (Leica

Microsystems Inc.). For HA affinity histochemistry the BOND Intense R Detection kit, a streptavidin-HRP system (Leica Microsystems, Inc.), was used with 4 μg/ml biotinylated HA-binding protein in 0.1% BSA-PBS as the primary. The BOND Polymer Detection Kit was used for all other immunohistochemistry. This detection kit contains a goat anti-rabbit conjugated to polymeric HRP and a rabbit anti-mouse post-primary reagent for use with mouse primaries.

For Foxp3 and insulin (anti-insulin; ab7842, Abcam) sections were incubated 60 min with 8 μg/ml rat anti-Foxp3 clone FJK-16s (eBioscience). Incubation with rabbit anti rat IgG (Vector Laboratories), post-primary was added in lieu of the post-primary reagent from the kit.

CD3 immune histochemistry required pretreatment using heat-mediated antigen retrieval with EDTA at high pH (BOND Epitope Retrieval Solution 2) for 20 min. Subsequently sections were incubated with 2.5 μg/ml rabbit anti-CD3 (A0452, Dako) and detection was performed using the BOND Polymer Refine Detection Kit.

All images were visualized using a Leica DMIRB inverted fluorescence microscope equipped with a Pursuit 4-megapixel–cooled color/monochrome charge-coupled device camera (Diagnostic Instruments). Images were acquired using the Spot Pursuit camera and Spot Advance Software (SPOT Imaging Solutions; Diagnostic Instruments). Image analysis was performed accordingly using ImageJ (National Institutes of Health), as described previously (17).

Mouse splenocyte isolation and regulatory T-cell identification

Collection of murine tissues and isolation of lymphocytes and splenocytes were performed as described previously (45). In brief, spleens were extracted from mice and cells were harvested by homogenization through a 70-μm cell strainer. Red blood cells were lysed using ammonium-chloride-potassium buffer. Splenocyte suspensions were stained and analyzed via flow cytometry using previously described protocols (11) and the following fluorochrome-conjugated antibodies: V500-CD3 (500A2), BV785-CD4 (RM4−5), and Al488-Foxp3 (FJK-16s). Flow cytometry was performed on an LSRII at the Stanford Shared FACS Facility and data analysis was done using FlowJo (Treestar).

RT-qPCR

RT-PCR for HAS1−3 was performed as described previously (30). In brief, cells and tissues were harvested for total RNA isolation using the High Pure RNA Isolation Kit (Roche Applied Science) and reverse transcribed using the High Capacity cDNA Reverse Transcription Kit (Applied Biosystems). For real-time quantitative PCR (RT-qPCR), all reagents were supplied by Applied Biosystems, unless otherwise noted. Relative quantification of HAS1, HAS2, and HAS3 gene expression was performed using TaqMan Gene Expression Assays HAS1 (Mm00468496_m1), HAS2 (Mm00515089_m1), HAS3 (Mm00515092_m1), respectively. Briefly, 100 ng cDNA was amplified in 1$\times$ TaqMan Gene Expression Master Mix with a 250 nM TaqMan probe in a 20 μl reaction. Melting curve analysis confirmed that only one product was amplified. Expression was normalized to actin. All reactions were run using the standard program for 50 cycles on an ABI 7900HT thermocycler. All samples were performed in triplicate, and copy number estimates were generated from a standard curve created by using a selected reference cDNA template and TaqMan probe.

Viability and ROS studies

CD4$^+$ T-cells were isolated via STEMCELL Technologies EasySep Mouse CD4$^+$ T-cell Isolation Kit (cat. 19852) from DO11.10 mice spleen and pooled lymph nodes. These were activated overnight (20 h) with 20 ng/ml PMA and 200 ng/ml ionomycin in a round-bottom 96-well plate in R10 media. Fifty thousand activated CD4$^+$ T-cells or U937 cells were plated for 24 h with 4-MU or 4-MUG at 300 μM or 100 μM. Cells were then stained with Annexin V APC (cat. 640920) for 15 min at room temperature in PBS supplemented with 2% FBS and 2.5 mM CaCl$_2$. Concurrently, the cells were stained with a Zombie Aqua Fixable Viability Kit (cat. 423102). Cells were washed twice with the calcium supplemented FACS buffer prior to fixation with 4% PFA for 10 min. Cells were washed once and resuspended in FACS buffer. To study ROS, the same treated cells were stained with CellROX Deep Red (cat. C10422). The cells were stained in 5 μM solution in R10 media for 30 min at 37 °C. Cells were washed once before Zombie Aqua viability staining prior to PFA fixation in the same manner as the Annexin V stain. After fixation, the cells were washed and resuspended in FACS buffer. Both groups of cells were analyzed on a Beckman Coulter Cytoflex and with FlowJo 10 software. Percent viability was determined as the percentage of singlet cells that were negative for Zombie Viability dye. Annexin V percentage was identified as the percentage of live singlet cells with signal above background levels. For the CellROX, geometric mean fluorescent intensity of live singlet cells was given.

2-Photon image analysis

2-Photon excitation uses two photons of longer wavelength to achieve the same energy as one photon, so fluorophore with known excitation peak at 405 nm would be excited at 810 nm by two photons. The treated and control animals were euthanized, and the different organs were enucleated, immediately secured in a specially designed chamber with PBS without fixation or manipulation, covered with a coverslip, and imaged with 2-photon microscope. Imaging of the tissue of interest was performed using an Ultima IV 2-photon microscope (Prairie Technologies) incorporating a pulsed laser (Deep See Mai Tai, Newport Corp.) with a tuning range of 690 to 1040 nm. The laser was tuned to 810 nm to excite 4-MU and dextran-TRITC within blood vessels. 4-MU signal was detected at the 460/50 nm emission filter and dextran-TRITC at 595/50 nm.

At excitation of 920 nm, collagen shows a distinct second harmonics signal at the 460/50 nm emission filter, whereas the signal of fluorophores such as 4-MU is undetectable at 920 nm excitation at the 460/50 nm emission filter. A water-immersion 20$\times$ (N.A. 0.95) objective (Olympus) was used. To create a typical Z-stack 80- to 100-μm-thick section, the tissue was scanned at 1 μm Z-steps at resolution of 1024 $\times$ 1024. Image analysis was performed using IMARIS software (Bitplane Inc.). Z stacks from two excitation wavelengths were merged into one

extended focus image, where second harmonics and 4-MU signal appear as separate channels.

Statistics

Data are expressed as mean $\pm$ S.E. of *n* independent measurements. The comparison between two groups was performed with unpaired *t* tests. The comparison between multiple groups was performed via one way analysis of variance (ANOVA) with Bonferroni post test *versus* control. A *p* value less than <0.05 was considered statistically significant. Data analysis was performed with the use of GraphPad Prism 5.0 software.

Study approval

All animal experiments and use procedures were approved by the Institutional Animal Care and Use Committee at Stanford University School of Medicine.

References

1. Fraser, J. R., Laurent, T. C., and Laurent, U. B. (1997) Hyaluronan: Its nature, distribution, functions and turnover. *J. Intern. Med.* **242,** 27–33 CrossRef Medline
2. Jiang, D., Liang, J., and Noble, P. W. (2011) Hyaluronan as an immune regulator in human diseases. *Physiol. Rev.* **91,** 221–264 CrossRef Medline
3. Termeer, C., Sleeman, J. P., and Simon, J. C. (2003) Hyaluronan—magic glue for the regulation of the immune response? *Trends Immunol.* **24,** 112–114 CrossRef Medline
4. Weigel, P. H., and DeAngelis, P. L. (2007) Hyaluronan synthases: A decade-plus of novel glycotransferases. *J. Biol. Chem.* **282,** 36777–36781 CrossRef Medline
5. Termeer, C., Benedix, F., Sleeman, J., Fieber, C., Voith, U., Ahrens, T., Miyake, K., Freudenberg, M., Galanos, C., and Simon, J. C. (2002) Oligosaccharides of hyaluronan activate dendritic cells via toll-like receptor 4. *J. Exp. Med.* **195,** 99–111 CrossRef Medline
6. Taylor, K. R., Trowbridge, J. M., Rudisill, J. A., Termeer, C. C., Simon, J. C., and Gallo, R. L. (2004) Hyaluronan fragments stimulate endothelial recognition of injury through TLR4. *J. Biol. Chem.* **279,** 17079–17084 CrossRef Medline
7. McKee, C. M., Penno, M. B., Cowman, M., Burdick, M. D., Strieter, R. M., Bao, C., and Noble, P. W. (1996) Hyaluronan (HA) fragments induce chemokine gene expression in alveolar macrophages. The role of HA size and CD44. *J. Clin. Invest.* **98,** 2403–2413 CrossRef Medline
8. Mahaffey, C. L., and Mummert, M. E. (2007) Hyaluronan synthesis is required for IL-2-mediated T cell proliferation. *J. Immunol.* **179,** 8191–8199 CrossRef Medline
9. Itano, N., Atsumi, F., Sawai, T., Yamada, Y., Miyaishi, O., Senga, T., Hamaguchi, M, and Kimata, K. (2002) Abnormal accumulation of hyaluronan matrix diminishes contact inhibition of cell growth and promotes cell migration. *Proc. Natl. Acad. Sci. U.S.A.* **99,** 3609–3614 CrossRef Medline
10. Bollyky, P. L., Falk, B. A., Long, S. A., Preisinger, A., Braun, K. R., Wu, R. P., Evanko, S. P., Buckner, J. H., Wight, T. N., and Nepom, G. T. (2009) CD44 costimulation promotes FoxP3$^+$ regulatory T cell persistence and function via production of IL-2, IL-10, and TGF-β. *J. Immunol.* **183,** 2232–2241 CrossRef Medline
11. Bollyky, P. L., Lord, J. D., Masewicz, S. A., Evanko, S. P., Buckner, J. H., Wight, T. N., and Nepom, G. T. (2007) Cutting edge: High molecular weight hyaluronan promotes the suppressive effects of CD4$^+$CD25$^+$ regulatory T cells. *J. Immunol.* **179,** 744–747 CrossRef Medline
12. Bollyky, P. L., Wu, R. P., Falk, B. A., Lord, J. D., Long, S. A., Preisinger, A., Teng, B., Holt, G. E., Standifer, N. E., Braun, K. R., Xie, C. F., Samuels, P. L., Vernon, R. B., Gebe, J. A., Wight, T. N., and Nepom, G. T. (2011) ECM components guide IL-10 producing regulatory T-cell (TR1) induction from effector memory T-cell precursors. *Proc. Natl. Acad. Sci. U.S.A.* **108,** 7938–7943 CrossRef Medline
13. Cheng, G., Swaidani, S., Sharma, M., Lauer, M. E., Hascall, V. C., and Aronica, M. A. (2011) Hyaluronan deposition and correlation with inflammation in a murine ovalbumin model of asthma. *Matrix Biol.* **30,** 126–134 CrossRef Medline
14. Kang, L., Lantier, L., Kennedy, A., Bonner, J. S., Mayes, W. H., Bracy, D. P., Bookbinder, L. H., Hasty, A. H., Thompson, C. B., and Wasserman, D. H. (2013) Hyaluronan accumulates with high-fat feeding and contributes to insulin resistance. *Diabetes* **62,** 1888–1896 CrossRef Medline
15. Mine, S., Okada, Y., Kawahara, C., Tabata, T., and Tanaka, Y. (2006) Serum hyaluronan concentration as a marker of angiopathy in patients with diabetes mellitus. *Endocr. J.* **53,** 761–766 CrossRef Medline
16. Bollyky, P. L., Bogdani, M., Bollyky, J. B., Hull, R. L., and Wight, T. N. (2012) The role of hyaluronan and the extracellular matrix in islet inflammation and immune regulation. *Curr. Diab. Rep.* **12,** 471–480 CrossRef Medline
17. Nagy, N., Kaber, G., Johnson, P. Y., Gebe, J. A., Preisinger, A., Falk, B. A., Sunkari, V. G., Gooden, M. D., Vernon, R. B., Bogdani, M., Kuipers, H. F., Day, A. J., Campbell, D. J., Wight, T. N., and Bollyky, P. L. (2015) Inhibition of hyaluronan synthesis restores immune tolerance during autoimmune insulitis. *J. Clin. Invest.* **125,** 3928–3940 CrossRef Medline
18. Hull, R. L., Johnson, P. Y., Braun, K. R., Day, A. J., and Wight, T. N. (2012) Hyaluronan and hyaluronan binding proteins are normal components of mouse pancreatic islets and are differentially expressed by islet endocrine cell types. *J. Histochem. Cytochem.* **60,** 749–760 CrossRef Medline
19. Kuipers, H. F., Rieck, M., Gurevich, I., Nagy, N., Butte, M. J., Negrin, R. S., Wight, T. N., Steinman, L., and Bollyky, P. L. (2016) Hyaluronan synthesis is necessary for autoreactive T-cell trafficking, activation, and Th1 polarization. *Proc. Natl. Acad. Sci. U.S.A.* **113,** 1339–1344 CrossRef Medline
20. Yoshioka, Y., Kozawa, E., Urakawa, H., Arai, E., Futamura, N., Zhuo, L., Kimata, K., Ishiguro, N., and Nishida, Y. (2013) Suppression of hyaluronan synthesis alleviates inflammatory responses in murine arthritis and in human rheumatoid synovial fibroblasts. *Arthritis Rheum.* **65,** 1160–1170 CrossRef Medline
21. Taylor, K. R., Yamasaki, K., Radek, K. A., Di Nardo, A., Goodarzi, H., Golenbock, D., Beutler, B., and Gallo, R. L. (2007) Recognition of hyaluronan released in sterile injury involves a unique receptor complex dependent on Toll-like receptor 4, CD44, and MD-2. *J. Biol. Chem.* **282,** 18265–18275 CrossRef Medline
22. Bollyky, P. L., Falk, B. A., Wu, R. P., Buckner, J. H., Wight, T. N., and Nepom, G. T. (2009) Intact extracellular matrix and the maintenance of immune tolerance: High molecular weight hyaluronan promotes persistence of induced CD4$^+$CD25$^+$ regulatory T cells. *J. Leukoc. Biol.* **86,** 567–572 CrossRef Medline
23. Garantziotis, S., Li, Z., Potts, E. N., Lindsey, J. Y., Stober, V. P., Polosukhin, V. V., Blackwell, T. S., Schwartz, D. A., Foster, W. M., and Hollingsworth, J. W. (2010) TLR4 is necessary for hyaluronan-mediated airway hyperresponsiveness after ozone inhalation. *Am. J. Respir. Crit. Care Med.* **181,** 666–675 CrossRef Medline
24. Hull, R. L., Bogdani, M., Nagy, N., Johnson, P. Y., and Wight, T. N. (2015) Hyaluronan: A mediator of islet dysfunction and destruction in diabetes? *J. Histochem. Cytochem.* **63,** 592–603 CrossRef Medline

ASBMB

25. Yung, S., and Chan, T. M. (2012) The role of hyaluronan and CD44 in the pathogenesis of lupus nephritis. *Autoimmune Dis.* **2012,** 207190 CrossRef Medline

26. Lee-Sayer, S. S., Dong, Y., Arif, A. A., Olsson, M., Brown, K. L., and Johnson, P. (2015) The where, when, how, and why of hyaluronan binding by immune cells. *Front. Immunol.* **6,** 150 CrossRef Medline

27. Jackson, D. G. (2009) Immunological functions of hyaluronan and its receptors in the lymphatics. *Immunol. Rev.* **230,** 216–231 CrossRef Medline

28. Petrey, A. C., and de la Motte, C. A. (2014) Hyaluronan, a crucial regulator of inflammation. *Front. Immunol.* **5,** 101 CrossRef Medline

29. Nagy, N., Kuipers, H. F., Frymoyer, A. R., Ishak, H. D., Bollyky, J. B., Wight, T. N., and Bollyky, P. L. (2015) 4-methylumbelliferone treatment and hyaluronan inhibition as a therapeutic strategy in inflammation, autoimmunity, and cancer. *Front. Immunol.* **6,** 123 CrossRef Medline

30. Bollyky, P. L., Evanko, S. P., Wu, R. P., Potter-Perigo, S., Long, S. A., Kinsella, B., Reijonen, H., Guebtner, K., Teng, B., Chan, C. K., Braun, K. R., Gebe, J. A., Nepom, G. T., and Wight, T. N. (2010) Th1 cytokines promote T-cell binding to antigen-presenting cells via enhanced hyaluronan production and accumulation at the immune synapse. *Cell Mol. Immunol.* **7,** 211–220 CrossRef Medline

31. Nagy, N., Freudenberger, T., Melchior-Becker, A., Röck, K., Ter Braak, M., Jastrow, H., Kinzig, M., Lucke, S., Suvorava, T., Kojda, G., Weber, A. A., Sörgel, F., Levkau, B., Ergün, S., and Fischer, J. W. (2010) Inhibition of hyaluronan synthesis accelerates murine atherosclerosis: Novel insights into the role of hyaluronan synthesis. *Circulation* **122,** 2313–2322 CrossRef Medline

32. Kakizaki, I., Kojima, K., Takagaki, K., Endo, M., Kannagi, R., Ito, M., Maruo, Y., Sato, H., Yasuda, T., Mita, S., Kimata, K., and Itano, N. (2004) A novel mechanism for the inhibition of hyaluronan biosynthesis by 4-methylumbelliferone. *J. Biol. Chem.* **279,** 33281–33289 CrossRef Medline

33. Kultti, A., Pasonen-Seppänen, S., Jauhiainen, M., Rilla, K. J., Kärnä, R., Pyöriä, E., Tammi, R. H., and Tammi, M. I.(2009) 4-Methylumbelliferone inhibits hyaluronan synthesis by depletion of cellular UDP-glucuronic acid and downregulation of hyaluronan synthase 2 and 3. *Exp. Cell Res.* **315,** 1914–1923 CrossRef Medline

34. Vigetti, D., Rizzi, M., Viola, M., Karousou, E., Genasetti, A., Clerici, M., Bartolini, B., Hascall, V. C., De Luca, G., and Passi, A. (2009) The effects of 4-methylumbelliferone on hyaluronan synthesis, MMP2 activity, proliferation, and motility of human aortic smooth muscle cells. *Glycobiology* **19,** 537–546 CrossRef Medline

35. Vigetti, D., Ori, M., Viola, M., Genasetti, A., Karousou, E., Rizzi, M., Pallotti, F., Nardi, I., Hascall, V. C., De Luca, G., and Passi, A. (2006) Molecular cloning and characterization of UDP-glucose dehydrogenase from the amphibian *Xenopus laevis* and its involvement in hyaluronan synthesis. *J. Biol. Chem.* **281,** 8254–8263 CrossRef Medline

36. Mueller, A. M., Yoon, B. H., and Sadiq, S. A. (2014) Inhibition of hyaluronan synthesis protects against central nervous system (CNS) autoimmunity and increases CXCL12 expression in the inflamed CNS. *J. Biol. Chem.* **289,** 22888–22899 CrossRef Medline

37. Takeda, S., and Aburada, M. (1981) The choleretic mechanism of coumarin compounds and phenolic compounds. *J. Pharmacobio-Dyn.* **4,** 724–734 CrossRef Medline

38. Garrett, E. R., Venitz, J., Eberst, K., and Cerda, J. J. (1993) Pharmacokinetics and bioavailabilities of hymecromone in human volunteers. *Biopharm. Drug Dispos.* **14,** 13–39 CrossRef Medline

39. Mulder, G. J., Brouwer, S., Weitering, J. G., Scholtens, E., and Pang, K. S. (1985) Glucuronidation and sulfation in the rat *in vivo*. The role of the liver and the intestine in the *in vivo* clearance of 4-methylumbelliferone. *Biochem. Pharmacol.* **34,** 1325–1329 CrossRef Medline

40. Kuipers, H. F., Nagy, N., Ruppert, S. M., Sunkari, V. G., Marshall, P. L., Gebe, J. A., Ishak, H. D., Keswani, S. G., Bollyky, J., Frymoyer, A. R., Wight, T. N., Steinman, L., and Bollyky, P. L. (2016) The pharmacokinetics and dosing of oral 4-methylumbelliferone for inhibition of hyaluronan synthesis in mice. *Clin. Exp. Immunol.* **185,** 372–381 CrossRef Medline

41. Vigetti, D., Viola, M., Karousou, E., De Luca, G., and Passi, A. (2014) Metabolic control of hyaluronan synthases. *Matrix Biol.* **35,** 8–13 CrossRef Medline

42. Berninsone, P., Hwang, H. Y., Zemtseva, I., Horvitz, H. R., and Hirschberg, C. B. (2001) SQV-7, a protein involved in *Caenorhabditis elegans* epithelial invagination and early embryogenesis, transports UDP-glucuronic acid, UDP-*N*-acetylgalactosamine, and UDP-galactose. *Proc. Natl. Acad. Sci. U.S.A.* **98,** 3738–3743 CrossRef Medline

43. Medina, C. O., Nagy, N., and Bollyky, P. L. (2018) Extracellular matrix and the maintenance and loss of peripheral immune tolerance in autoimmune insulitis. *Curr. Opin. Immunol.* **55,** 22–30 CrossRef Medline

44. Coulson-Thomas, V., and Gesteira, T. (2014) Dimethylmethylene blue assay (DMMB). *Bio-protocol* **4,** e1236 CrossRef

45. Ruppert, S. M., Falk, B. A., Long, S. A., and Bollyky, P. L. (2015) Regulatory T cells resist cyclosporine-induced cell death via CD44-mediated signaling pathways. *Int. J. Cell Biol.* **2015,** 614297 CrossRef Medline

SASBMB

J. Biol. Chem. (2019) 294(19) 7864–7877 **7877**